optica

Disorder-induced high-quality wavefront in an Anderson localizing optical fiber

Behnam Abaie,[1,2] Mostafa Peysokhan,[1,2] Jian Zhao,[3] Jose E. Antonio-Lopez,[3] Rodrigo Amezcua-Correa,[3] Axel Schülzgen,[3] and Arash Mafi[1,2,*]

[1]Department of Physics & Astronomy, University of New Mexico, Albuquerque, New Mexico 87131, USA
[2]Center for High Technology Materials (CHTM), University of New Mexico, Albuquerque, New Mexico 87106, USA
[3]CREOL, College of Optics and Photonics, University of Central Florida, Orlando, Florida 32816, USA
*Corresponding author: mafi@unm.edu

Received 26 March 2018; revised 15 July 2018; accepted 19 July 2018 (Doc. ID 326665); published 8 August 2018

High-quality coherent wavefronts are extremely useful in optical communications and lasers. Disorder is usually considered as a source of noise and deviation from ideal designs for generating high-quality beams in photonic devices. Here, we demonstrate that strong disorder can be exploited to obtain high-quality wavefronts thanks to the Anderson localization phenomenon. Our analysis on a transverse Anderson localizing optical fiber reveals that a considerable number of the guided modes have $M^2 < 2$ values. These high-quality modes are distributed across the transverse profile of the disordered fiber and can be excited without requiring sophisticated spatial light modulations at the input facet. The results show the potential of such fibers for novel applications in fiber lasers and nonlinear devices, where a high beam quality is desirable.

OCIS codes: (290.4210) Multiple scattering; (140.3295) Laser beam characterization; (030.1640) Coherence; (060.2430) Fibers, single-mode.

https://doi.org/10.1364/OPTICA.5.000984

High-quality single-mode or diffraction-limited beams are of significant importance in lasers [1] and optical communications [2]. Laser beam quality is critical in a variety of applications, including material processing and nonlinear optics. An effective method to enhance beam quality and obtain a nearly diffraction-limited laser beam is to pass the light through a "long enough" single-mode optical fiber [3]. Combination of the long amplification lengths and high beam qualities, provided by various forms of active single-mode fibers, has enabled significant power scaling in laser technology [4].

Transverse Anderson localization (TAL) [5–9] has recently fostered a new class of disordered waveguides, in which strong transverse confinement mediated by Anderson-localized modes balances the diffraction of light as it propagates freely along the waveguide [10–13]. In a recent study, it has been shown that localized modes of a disordered fiber can be exploited for single-mode transmission [14]. TAL optical fibers (TALOFs) have already been successfully used for image transport [15,16] and making directional and highly stable random fiber lasers [17]. For use in optical communications, the modal and chromatic dispersion properties of the localized modes should be studied in detail. The rich spectral properties of these fibers also hint at their potential applications in cavity quantum electrodynamics [18], optical sensing [19], and wavelength division multiplexing [14].

In this Letter, we evaluate the beam quality of highly localized modes in a glass-TALOF. It is shown that a high degree of wavefront quality can be obtained due to the disorder-induced Anderson localization. A large number of localized modes exhibit $M^2 < 2$ values, which is indicative of nearly diffraction-limited beam qualities. We start by evaluating the beam quality of 1500 numerically calculated localized modes in the disordered fiber and observe the presence of high-quality modes at various locations across the transverse profile of the fiber. Highly localized modes are then experimentally excited in the disordered fiber. An experimental evaluation of the beam quality of the localized modes proves the validity of our numerical predictions. Finally, we use a high-quality localized beam at the output of the disordered fiber in a Young double-slit experiment and show that the spatial coherence of the localized mode is comparable to that of a high-quality wavefront extracted from a single-mode optical fiber.

Glass-TALOF used in this work is fabricated at the University of Central Florida using silica rods and tubes in a stack-and-draw approach [16]. A scanning electron microscope (SEM) image of the fiber and a magnified version are shown in Fig. 1(a) and Fig. 1(b), respectively. The dark sites are representative of the air-holes, which remain the same along the disordered fiber [20]. Transverse randomness of the refractive index profile results in strong scattering and therefore TAL.

Figure 2(a) shows a numerically calculated localized mode in the fiber using the finite element method (FEM). The geometry of the fiber is directly extracted from the SEM image and imported to COMSOL. The mode is calculated at $\lambda = 632.8$ nm, the wavelength of HeNe laser used for the experiments. The calculated mode demonstrated in Fig. 2(a) is numerically propagated along the z direction in free space using a Fast Fourier Transform

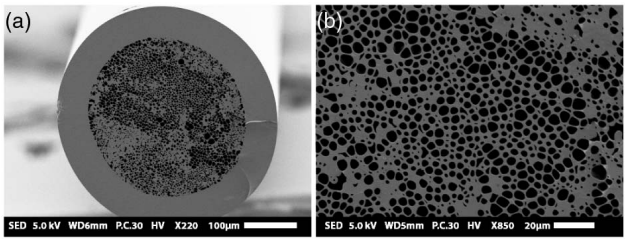

Fig. 1. (a) SEM image of the tip of glass-TALOF. The darker sites are the air-holes. (b) Magnified SEM image shows the details of the air-holes in a portion of the fiber cross section.

algorithm. The beam waist across the rectangular coordinate $x(y)$ is calculated by $w_x = 2\sigma_x$ ($w_y = 2\sigma_y$) where σ_x (σ_y) is the standard deviation of mode intensity profile:

$$\sigma_x^2 = \int \mathrm{d}\mathcal{A}(x-\bar{x})^2 I(x,y), \qquad \sigma_y^2 = \int \mathrm{d}\mathcal{A}(y-\bar{y})^2 I(x,y) \tag{1}$$

$$\bar{x} = \int \mathrm{d}\mathcal{A} x I(x,y), \quad \bar{y} = \int \mathrm{d}\mathcal{A} y I(x,y), \tag{2}$$

where $\int \mathrm{d}\mathcal{A} \equiv \iint \mathrm{d}x\mathrm{d}y$, $(\bar{x},\bar{y})$ represents the mode center coordinates and $\int \mathrm{d}\mathcal{A} I(x,y) = 1$. The value of M_x^2 and M_y^2 are extracted using the variance method (see Section 1 in Supplement 1 for details) [21–23]. Figure 2(b) shows M^2 values for this mode along the x and y coordinates. M_x^2, $M_y^2 \sim 1$ is indicative of the nearly diffraction-limited beam quality of the localized mode.

Glass-TALOF supports a large number of guided modes; this number (N) can be estimated using the V parameter:

$$N \approx \frac{V^2}{2}, \qquad \text{where } V = \frac{2\pi a}{\lambda}\sqrt{n_2^2 - n_1^2}. \tag{3}$$

Here, $a = 140$ μm is the radius of the fiber, and $n_2 = 1.46$ and $n_1 = 1$ are the refractive indexes of silica and air (cladding), respectively. For $\lambda = 632.8$ nm, the total number of the modes is $N \gtrapprox 10^6$. Therefore, a statistical approach is warranted to get an understanding of the beam quality properties of the guided modes in this fiber [24–29]. The guided modes of the disordered fiber have a broad range of transverse spatial frequencies (k_T), nominally in the range of $0 < k_T \lessapprox V/(n_2 a)$. In this Letter, our main focus is to establish the presence of modes with low M^2 values, which are broadly associated with low values of k_T: such modes are primarily excited in our experimental setup, which uses a regular Gaussian-like beam from a single-mode optical fiber. As such, our simulations also target modes with large propagation constants that naturally correspond to low values of k_T. We emphasize that "highly localized" Anderson-localized modes can come with both low k_T or high k_T values, as shown in Refs. [9,30,31], but our focus is on the presence of low k_T high-propagation-constant modes, which also correspond to low M^2 values. We emphasize that each localized mode, regardless of its shape and form, is Anderson-localized due to the presence of the strong disorder. However, if one desires to verify the Anderson localization using the common signature of the exponential decay, the log-averaging must be performed over all of the modes, as shown in Ref. [11], rather than a subset.

In the following, we consider 1000 modes with the largest effective refractive index (all calculated at $\lambda = 632.8$ nm) corresponding to the lowest transverse spatial frequencies. Figure 2(c) shows a histogram of numerically calculated M_x^2 values for 1000 localized modes with the highest effective refractive index values. The vertical axis is the number of modes that correspond to the relevant M_x^2 on the horizontal axis. Based on this result, although the modes with an $M^2 < 2$ peak in the histogram, they are not statistically dominant in the entire landscape of fiber modes. A density histogram of the transverse position of the calculated localized modes in Fig. 2(c) is shown in Fig. 2(d). The transverse position of the modes are calculated from Eq. (2). The value of each pixel in Fig. 2(d) is the number of localized modes, such that the sum of all pixel values is equal to 1000; the distribution of the modes is nonuniform.

The results shown in Figs. 2(c) and 2(d) may appear to contradict the experimental results presented later in this Letter, where the single-mode channels are abundant and can be easily excited. The answer to this puzzling situation is that we have been solving for the modes with the highest effective refractive index (otherwise the total number of modes would be enormous), because of the limited numerical aperture of the launch fiber. However, it appears that the nonuniform air fill-fraction in Fig. 1(a) biases our results towards regions with low air-hole density, over which the hot areas appear in the sparse density histogram in Fig. 2(d).

In order to prove this observation and mitigate the aforementioned bias, we manage to solve for the modes located in the regions with a higher density of air-holes. For accomplishing this goal, we choose five separate circular domains with a radius around $r \approx 35$ μm and calculate modes in these domains (see Section 2 in Supplement 1 for details). We add the M_x^2 of 100 modes from each domain to the previous ensemble shown

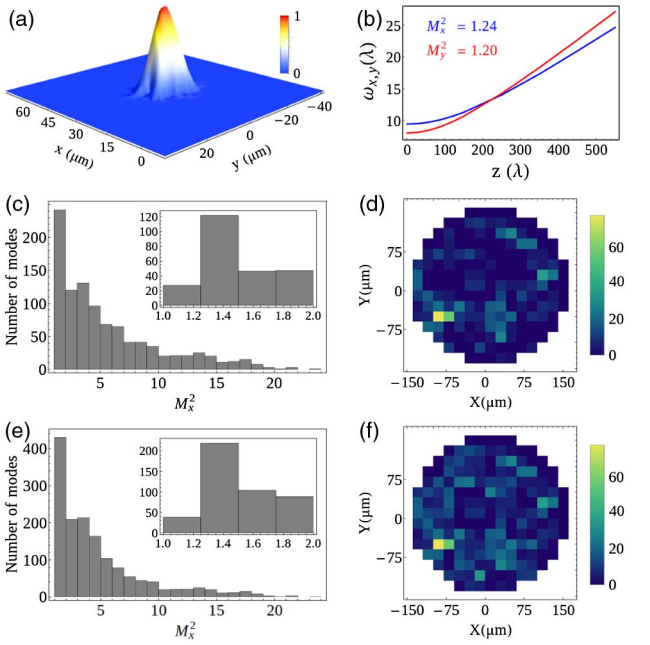

Fig. 2. (a) Numerically calculated mode and (b) its M^2 values in x and y coordinates. (c) Histogram of the calculated M_x^2 for 1000 localized modes. (d) Density histogram representative of the location of the modes. (e) The same as part c in the presence of an additional 500 calculated modes. (f) Density histogram representative of the location of the modes in part e.

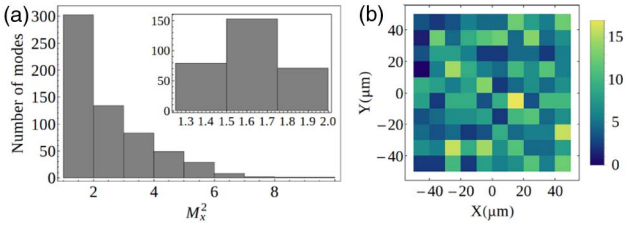

Fig. 3. (a) Histogram of M_x^2 values for a TALOF with optimal parameters. (b) Density histogram of the mode locations. Modes are distributed uniformly across the transverse profile of the disordered fiber.

in Fig. 2(d) and plot the histogram of the new ensemble in Fig. 2(e): the histogram clearly shows that several high-quality modes are added to the statistical ensemble compared to Fig. 2(c). The $M^2 < 2$ modes are even more probable in these regions due to the fact that the air fill-fraction is larger in the added computational domains, and, therefore, the localization is stronger in them, which is directly causing the presence of more high-quality wavefronts in them. Apparently, Fig. 2(f) is indicative of a more uniform mode distribution because modes from the five domains, which were absent in Fig. 2(c), are added in this figure.

In order to further investigate the impact of the air fill-fraction, both in terms of the participation ratio and uniformity, we show the simulation results related to a TALOF with optimal design parameters from Ref. [20] in the following. The refractive index contrast is kept the same but a 50% fill-fraction is used (see Section 2 in Supplement 1 for details). Figures 3(a) and 3(b) show the histogram of M_x^2 values for nearly 500 localized modes and the distribution of them across the profile of the fiber, respectively. The uniformity of the air fill-fraction not only improves the distribution of the modes, but also increases the localization strength and, therefore, the quality of the modes; $M_x^2 < 2$ modes are quite dominant in Fig. 3(a).

In the following, we manage to excite localized modes of glass-TALOF in an experimental setup and evaluate their beam quality values using the variance method (see Section 1 in Supplement 1 for details) [21–23]. The output of a HeNe laser is coupled into a single-mode optical fiber (*ThorlabsSM400*) and directly butt-coupled into a 155 cm long segment of glass-TALOF. The launch transverse position is scanned accurately across its input facet (see Section 3 in Supplement 1 for details).

Figure 4 shows the beam profile of two experimentally excited localized modes. The localized modes highly resemble the numerically calculated mode in Fig. 2(a). The corresponding M^2 values in the x and y coordinates are also demonstrated in Fig. 4. Excellent $M^2 < 2$ values prove the nearly diffraction-limited beam profiles of the localized modes. A histogram of M^2 values for 30 localized modes in the x and y coordinates are shown in Figs. 5(a) and 5(b), respectively. The majority of the modes show $M^2 < 2$.

It is critical to note that the highly localized modes are excited easily by probing the launch fiber across the facet of glass-TALOF. The disordered fiber contains a large number of modes, many of which have high beam quality and many do not. The extremely large number of modes in such a fiber (more than a million) guarantees that high-beam-quality modes are abundant and distributed over the entire transverse profile of the fiber.

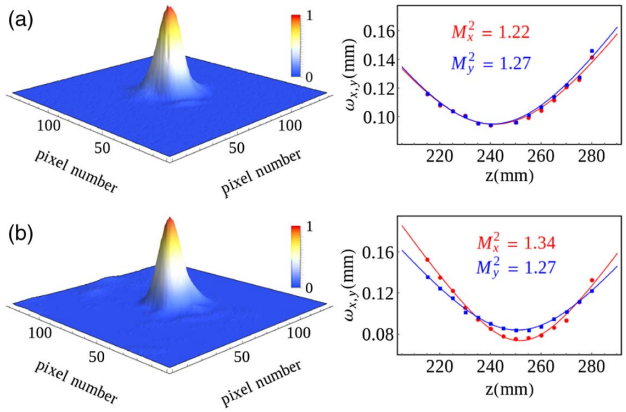

Fig. 4. (a) and (b) Two experimentally exited modes and their M^2 values in the x and y coordinates. M_x^2, $M_y^2 \sim 1$ are indicative of nearly diffraction-limited beam quality of the localized modes.

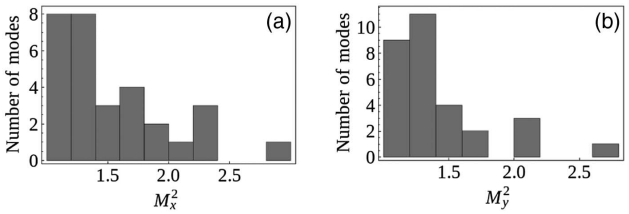

Fig. 5. Histogram of M^2 evaluated for 30 localized modes in the (a) x coordinate and (b) y coordinate. Several modes have $M^2 < 2$.

The disordered fiber studied here is a highly multimode fiber, naturally, as it possesses several thousands of modes due to its large transverse size. The main difference between glass-TALOF and conventional multimode fibers is that the modes are spatially isolated due to TAL. A direct advantage of this distinction is that each mode can be easily excited without assistance of expensive and sophisticated spatial light modulators [14]. Moreover, a large number of the localized modes can feature a high degree of wavefront quality as a direct consequence of spatial confinement provided by TAL, similar to single-mode fibers [14].

A unique feature of high-quality wavefronts is their degree of spatial coherence; a wavefront that contains several modes results in a speckle pattern, whereas single modes exhibit a high degree of spatial coherence [32]. In the following, we investigate spatial coherence of a localized mode. Figure 6(a) shows the experimental setup used for this purpose. The output of glass-TALOF is collected by a 60 times objective and used to illuminate the double slit of width 80 μm and with 500 μm center-to-center spacing. The interference pattern is recorded by a CCD beam profiler. Figures 6(c) and 6(d) are the interference pattern generated by the mode in Fig. 6(b) and the intensity distribution averaged over all vertical lines in the interference pattern, respectively. Clearly, the localized beam forms a clear interference fringe at the far-field, indicative of high spatial coherence of the beam.

In their pioneering work, Ballato's group at Clemson University fabricated the first reported glass-TALOF from a porous glass preform [33], and the fiber was later used for the analysis of the spatial coherence of the localized modes [34].

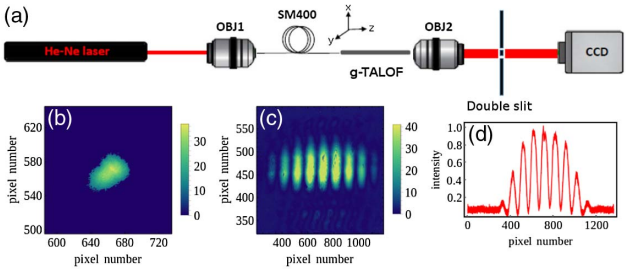

Fig. 6. (a) Experimental setup for spatial coherence measurement: a localized mode is excited, and the beam at the output of the glass-TALOF is used in a Young double-slit setting. (b) The localized beam profile used for spatial coherence evaluation. (c) Interference pattern generated by the localized mode. (d) Intensity distribution averaged over all vertical lines in the interference pattern of part c.

A weaker disorder and TAL resulted in a relatively washed out interference pattern, which can be attributed to the simultaneous excitation of extended modes along with localized ones [34]. The stronger TAL in the glass-TALOF used in this study enables excitation of individual localized modes and, therefore, a higher degree of spatial coherence. Stronger TAL in the glass-TALOF used here is a result of higher air fill-fraction in the fiber. In the previous glass-TALOF, the air fill-fraction ranged between 2% and 7% depending on the transverse location, whereas the glass-TALOF used here has ~20% air fill-fraction and, therefore, a much stronger transverse disorder. The ideal fill-fraction to optimize localization strength is 50% [20] (see Section 2 in Supplement 1 for details).

In conclusion, we presented our numerical and experimental study on wavefront quality of a subset of the localized modes possessing the lowest transverse momentum in a disordered optical fiber. The analyzed guided modes demonstrate $M^2 < 2$ values and are distributed across the tip of the fiber. We experimentally excited the high-quality localized modes and evaluated their M^2 values at the output. The results confirm our numerical study. The localized modes also present a high degree of spatial coherence similar to the output of single-mode fibers. Therefore, nearly diffraction-limited beam qualities are obtained in the disordered medium. Application of these high-quality modes along with recent advances in TALOF lasers [17] can foster a new class of single-mode fiber lasers.

Acknowledgment. We are thankful to the UNM Center for Advanced Research Computing for providing access to computational resources and Mahmoud Behzadirad for the SEM images.

See Supplement 1 for supporting content.

REFERENCES

1. A. E. Siegman, *Lasers* (Technology & Engineering, 1986).
2. S. Miller, *Optical Fiber Telecommunications* (Elsevier, 2012).
3. O. Wallner, W. R. Leeb, and P. J. Winzer, J. Opt. Soc. Am. A **19**, 2445 (2002).
4. C. Jauregui, J. Limpert, and A. Tünnermann, Nat. Photonics **7**, 861 (2013).
5. H. De Raedt, A. Lagendijk, and P. de Vries, Phys. Rev. Lett. **62**, 47 (1989).
6. S. Abdullaev and F. K. Abdullaev, Radiofizika **23**, 766 (1980).
7. T. Schwartz, G. Bartal, S. Fishman, and M. Segev, Nature **446**, 52 (2007).
8. M. Segev, Y. Silberberg, and D. N. Christodoulides, Nat. Photonics **7**, 197 (2013).
9. A. Mafi, Adv. Opt. Photon. **7**, 459 (2015).
10. S. Karbasi, C. R. Mirr, P. G. Yarandi, R. J. Frazier, K. W. Koch, and A. Mafi, Opt. Lett. **37**, 2304 (2012).
11. S. Karbasi, K. W. Koch, and A. Mafi, J. Opt. Soc. Am. B **30**, 1452 (2013).
12. B. Abaie, S. R. Hosseini, S. Karbasi, and A. Mafi, Opt. Commun. **365**, 208 (2016).
13. B. Abaie and A. Mafi, Phys. Rev. B **94**, 064201 (2016).
14. G. Ruocco, B. Abaie, W. Schirmacher, A. Mafi, and M. Leonetti, Nat. Commun. **8**, 14571 (2017).
15. S. Karbasi, R. J. Frazier, K. W. Koch, T. Hawkins, J. Ballato, and A. Mafi, Nat. Commun. **5**, 3362 (2014).
16. J. Zhao, J. E. A. Lopez, Z. Zhu, D. Zheng, S. Pang, R. A. Correa, and A. Schülzgen, Sci. Rep. **8**, 3065 (2018).
17. B. Abaie, E. Mobini, S. Karbasi, T. Hawkins, J. Ballato, and A. Mafi, Light Sci. Appl. **6**, e17041 (2017).
18. L. Sapienza, H. Thyrrestrup, S. Stobbe, P. D. Garcia, S. Smolka, and P. Lodahl, Science **327**, 1352 (2010).
19. O. J. Trojak, T. Crane, and L. Sapienza, Appl. Phys. Lett. **111**, 141103 (2017).
20. S. Karbasi, C. R. Mirr, R. J. Frazier, P. G. Yarandi, K. W. Koch, and A. Mafi, Opt. Express **20**, 18692 (2012).
21. A. E. Siegman, in *Diode Pumped Solid State Lasers: Applications and Issues* (Optical Society of America, 1998), paper MQ1.
22. A. Mafi and J. V. Moloney, J. Lightwave Technol. **23**, 2267 (2005).
23. L. Li, A. Schülzgen, V. Temyanko, T. Qiu, M. Morrell, Q. Wang, A. Mafi, J. Moloney, and N. Peyghambarian, Opt. Lett. **30**, 1141 (2005).
24. A. Chabanov, M. Stoytchev, and A. Genack, Nature **404**, 850 (2000).
25. T. Pertsch, U. Peschel, J. Kobelke, K. Schuster, H. Bartelt, S. Nolte, A. Tünnermann, and F. Lederer, Phys. Rev. Lett. **93**, 053901 (2004).
26. P. Sebbah, B. Hu, J. M. Klosner, and A. Z. Genack, Phys. Rev. Lett. **96**, 183902 (2006).
27. J. Wang and A. Z. Genack, Nature **471**, 345 (2011).
28. A. P. Mosk, A. Lagendijk, G. Lerosey, and M. Fink, Nat. Photonics **6**, 283 (2012).
29. M. Koirala, R. Sarma, H. Cao, and A. Yamilov, Phys. Rev. B **96**, 054209 (2017).
30. R. G. S. El-Dardiry, S. Faez, and A. Lagendijk, Phys. Rev. B **86**, 125132 (2012).
31. Y. Lahini, A. Avidan, F. Pozzi, M. Sorel, R. Morandotti, D. N. Christodoulides, and Y. Silberberg, Phys. Rev. Lett. **100**, 013906 (2008).
32. M. Dzhibladze, B. Lezhava, and T. Y. Chelidze, Soviet J. Quantum Electron. **4**, 1181 (1975).
33. S. Karbasi, T. Hawkins, J. Ballato, K. W. Koch, and A. Mafi, Opt. Mater. Express **2**, 1496 (2012).
34. B. Abaie, T. Hawkins, J. Ballato, and A. Mafi, in *Laser Science* (Optical Society of America, 2017), paper JW4A-96.